31st Annual International Conference of the IEEE EMBS
Minneapolis, Minnesota, USA, September 2-6, 2009

Multimodal Optical Molecular Image Reconstruction with Frequency Domain Measurements

M. Bartels*, W. Chen*, R. Bardhan†, S. Ke*, N. J. Halas†, T. Wareing††, J. McGhee††, and A. Joshi*[1]

***Abstract*— Multimodality molecular imaging is becoming more and more important to understand both the structural and the functional characteristics of tissue, organs and tumors. So far, invasive nuclear methods utilizing ionizing radiation have been the "gold standard" of molecular imaging. We investigate non-contact, non-invasive, patient-tolerant and inexpensive near infrared (NIR) frequency domain optical tomography (FDOT) as a functional complement to structural X-ray computed tomography (CT) data. We show a novel multifrequency NIR FDOT approach both in transmission and reflectance mode and employ radiative transport equation (RTE) for 3D reconstruction of a target with novel fluorescent gold nanoshell indocyanine green (NS ICG) in an *ex vivo* nude mouse. The results demonstrate that gold NS ICG with multifrequency NIR FDOT is a promising fluorophore for multimodal optical molecular image reconstruction.**

I. Introduction

Multimodal imaging plays an important role in capturing not only the anatomical features of a patient but also the functionality of organs, tumors and tissue. Imaging modalities such as X-ray computed tomography (CT) offer structural insight into a body however lack an answer to the latter. Positron emission tomography (PET) and single photon emission computed tomography (SPECT) are widely accepted among physicians for imaging tissue functionality due to high sensitivity and penetration depths of tissue. However, repetitive use of these "gold standard" techniques is limited due to restricted exposure to patients.

Near infrared (NIR) fluorescence frequency domain optical tomography (FDOT) promises highly sensitive imaging of cancer metastasis in lymph nodes. It is non-invasive, does not utilize ionizing radiation and is inexpensive compared to nuclear isotope-based molecular imaging such as PET and SPECT. Patterned excitation based tomography is suited for scanning large tissue surfaces for staging breast cancer and melanoma [1] and can be repeatedly employed since current NIR imaging is not limited in dose. It is easy to implement in a clinical environment and is comfortable for patients due to non-contact data acquisition. Homodyne measurements in FD allows measuring amplitude and phase of fluorescent targets as opposed to diffuse continuous wave (CW) measurements. Although often neglected, the use of multiple modulation frequencies is promising since Milstein *et. al.* [2] have shown that multiple frequencies can improve image quality for well-localized objects.

In this paper, we present an *ex vivo* small animal study to demonstrate multimodal optical molecular image reconstruction using NIR FDOT and X-ray CT. To the best of our knowledge, this novel approach shows for the first time multifrequency FDOT with gold nanoshell indocyanine green (NS ICG) in transmission and reflectance mode. The remaining paper is organized as follows. Section II presents material and methods, section III develops the theory of radiative transport equation (RTE) based fluorescence tomography. Section IV presents results and discussion on the reconstructed multimodal molecular imagery. Section V concludes the paper and points out future research avenues.

II. Materials and Methods

A. NIR Multiple Frequency Domain Optical Tomography

Fig. 1 depicts the setup for an automated NIR FDOT system for homodyne measurements. The novelty of our system is the ability to image at multiple frequencies in both transmission a) or reflectance b) mode. In transmission mode a laser point source and camera are separated by the animal as opposed to reflectance mode where a diffused laser source is shone onto the animal facing the camera. The main component of the system is a gain controlled intensified charge-coupled device (ICCD, PI-MAX II, Princeton Instruments), consisting of photo cathode, multi-channel plate (MCP) and intensifier which are internally coupled to the CCD with optical fibers. We use a 28 mm Nikkor (Nikon)

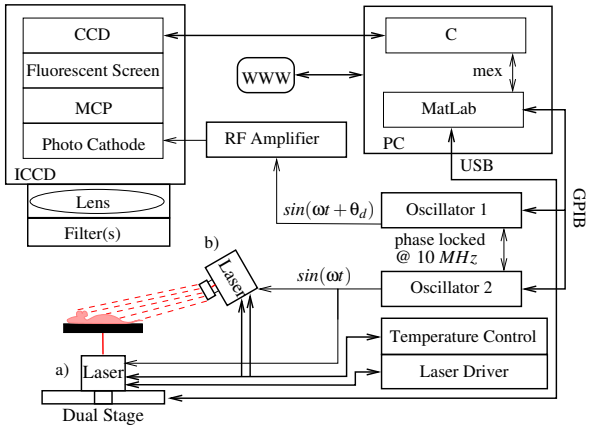

Fig. 1. Near infrared frequency domain optical tomography for a) transmission or b) reflectance mode.

*Department of Radiology, Baylor College of Medicine, One Baylor Plaza, 77030 Houston, Texas, USA
†Department of Chemistry, Rice University, 6100 Main Street, MS 60, Houston, Texas 77005, USA
‡Department of Mathematics, Texas A&M University, MS 3368, College Station, Texas 77843, USA
‡‡Transpire Inc., 6659 Kimball Drive, Suite E502, Gig Harbor, Washington 98335, USA
[1]Corresponding author: amitj@bcm.edu

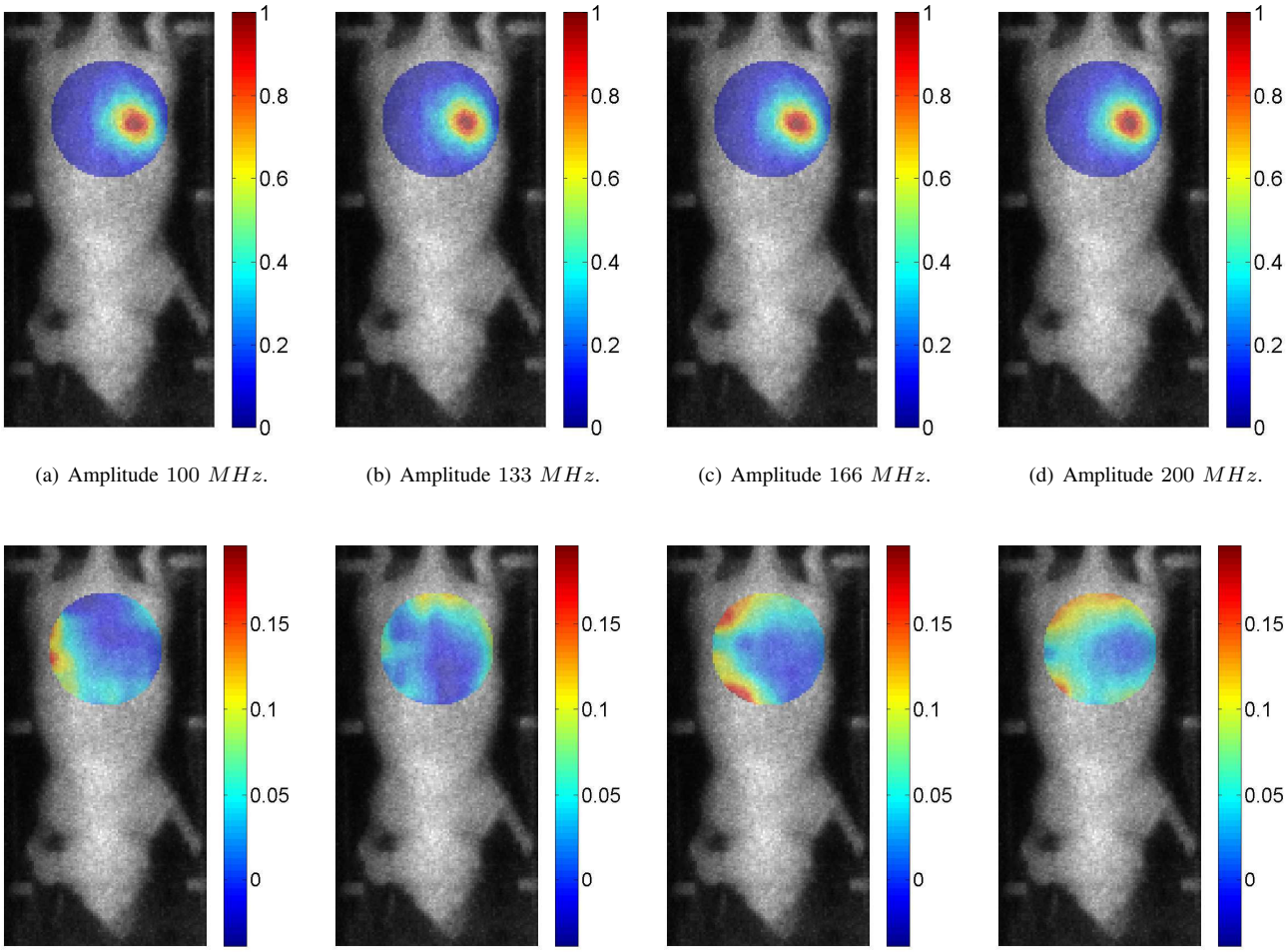

(a) Amplitude 100 MHz. (b) Amplitude 133 MHz. (c) Amplitude 166 MHz. (d) Amplitude 200 MHz.

(e) Phase 100 MHz. (f) Phase 133 MHz. (g) Phase 166 MHz. (h) Phase 200 MHz.

Fig. 2. Amplitude and phase of diffuse reflectance mode at $f = [100, 133, 166, 200]\ MHz$.

lense and appropriate neutral density filters with optical densities (OD) 3, 4 (Andover Corporation) and 6 (Thorlabs, Inc.) for collecting excitation light from a 100 mW NIR diode at 785 nm (Thorlabs, Inc.). A fluorescence band pass filter at 810 nm (CVI Laser, LCC) and a holographic notch filter at 785 nm (Kaiser Optical Systems, Inc.) is used for collecting emission light while rejecting potential excitation leakage, as suggested by Hwang *et. al.* [3]. The intensifier is modulated with an amplified (ENI 604L 4W) sinusoidal signal $sin(\omega t + \theta_d)$ from oscillator 1 (PTS 310) while being phase-locked with oscillator 2 (Marconi 2022D) which modulates the laser source at the same frequency $sin(\omega t)$ shifted by a variable phase delay θ_d, as proposed by Reynolds *et. al.* [4]. Using the programmable PTS 310, a sine wave is fit into a stack of $d \in (1..2^n)$, $d \in \mathbb{N}$, $n \in \mathbb{N}$ phase delayed images, where Fast Fourier Transform (FFT) yields real and imaginary components for further analysis. Central controlling unit is a standard personal computer (Dell PC, Intel Xeron, 2.33 GHz, 2.35 GB RAM) which controls ICCD, both oscillators via General Purpose Interface Bus (GPIB), and the step motorized nanometer dual translation stage (Thorlabs, Inc.) via universal serial bus (USB) when run in transmission mode a). The NIR FDOT system is fully automated and network controlled allowing the whole setup to be in a dark room. The user is informed via email once the experiment is conducted.

B. Gold Nanoshell Indocyanine Green

Indocyanine green (ICG), the only United Stated (US) Food and Drug Administration (FDA) approved NIR emitting fluorophore, is frequently utilized for biomedical imaging [5]. However, ICG has a low quantum yield of only $\sim 1.3\ \%$ in aqueous media [6] and is prone to instability and photo bleaching [7]. Recently, Bardhan *et. al.* [8] demonstrated that the emission of weak fluorophores such as ICG as well as IR800 can be enhanced $40 - 50$-fold, and nearly $86\ \%$ quantum efficiency can be achieved when placed in proximity to gold nanoshells (NS) at a distance of a few nanometers from the NS surface [9]. For this study, we have employed NS ICG at a concentration of 500 nM in H_2O, $3 \times 10^9\ part/ml$.

C. Data Registration for Multimodal Imaging

Multimodal imaging combining optical and nuclear measurements requires materials that are suitable for both modalities. For imaging with a NIR OT system and a CT scanner, a mouse holding bed in Fig. 2 is designed with SolidWorks. The bed is composed of three pieces: an opaque frame made of black delrin to deter undesired reflected light hitting the animal, a transparent clear lexan plate mounted below the animal to account for NIR light and adjustable white silicon fiducial screws. The frame has two additional holes to allow anesthesia tubes to enter the bed at the front and the mouse tail to exit the bed at its rear, respectively. This is especially important for *in vivo* studies where the fluorescent dye is injected into the tail vein.

For solving RTE model based fluorescence tomography, as developed by Joshi *et. al.* [10], co-registration of functional OT and structural X-ray CT data (Siemens MicroCAT™II) is necessary. Fiducials provide common geometrical coordinates for both planes. OT CCD data is treated as projections of true measurements on the animal surface. It is registered with the triangular boundary faces of the animal body mesh derived from CT data, as segmented and meshed in the visualization environment AMIRA.

III. RTE BASED FLUORESCENCE TOMOGRAPHY

For brevity, we write the coupled frequency domain excitation and emission RTE as a block linear system:

$$\begin{bmatrix} H_x & 0 \\ -B_{xm} & H_m \end{bmatrix} \begin{bmatrix} \widetilde{\Phi}_x \\ \widetilde{\Phi}_m \end{bmatrix} = \begin{bmatrix} S_{ex} \\ 0 \end{bmatrix} \tag{1}$$

$$H_{x,m} = \mathbf{\Omega} \cdot \nabla \widetilde{\Phi}_{x,m} + \left[\Sigma_T^{x,m}(\mathbf{r}) + \frac{i\omega}{c_{x,m}} \right] - Q_{scat}^{x,m} \tag{2}$$

$$B_{xm}\widetilde{\Phi}_x = \frac{1}{4\pi} \int_{4\pi} \frac{\eta(\mathbf{r})}{1 + i\omega\tau(\mathbf{r})} \widetilde{\Phi}_x(\mathbf{r}, \mathbf{\Omega}, \omega) d\mathbf{\Omega} \tag{3}$$

$$Q_{scat}^{x,m} = \mu_s^{x,m}(\mathbf{r}) \int_{4\pi} p(\mathbf{\Omega} \cdot \mathbf{\Omega}') \widetilde{\Phi}_{x,m}(\mathbf{r}, \mathbf{\Omega}', \omega) d\mathbf{\Omega}' \tag{4}$$

$$\Sigma_T^{x,m}(\mathbf{r}) = \mu_s^{x,m}(\mathbf{r}) + \mu_{ai}^{x,m}(\mathbf{r}) + \mu_{af}^{x,m}(\mathbf{r}) \tag{5}$$

$$\eta(\mathbf{r}) = \nu(\mathbf{r}) \mu_{af}^{x}(\mathbf{r})$$

Here H denotes the transport operator, subscripts x, m represent excitation and emission wavelengths respectively. B_{xm} is the term coupling the excitation RTE with the emission RTE and it depends upon the quantum yield $(\nu(\mathbf{r})\mu_{af}^{x}(\mathbf{r}))$ and the lifetime $\tau(\mathbf{r})$ of the fluorescence probe employed. The NIR light transport in tissue is governed by the absorption μ_a and scattering μ_s cross-sections. Subscript i denotes the properties of endogenous chromophores, while subscript f denotes the properties of exogenous fluorophores. $Q_{scat}^{x,m}$ is the scattering source which depends upon the probability $p(\mathbf{\Omega} \cdot \mathbf{\Omega}')$ of scattering of a photon from the direction $\mathbf{\Omega}$ to $\mathbf{\Omega}'$. S_{ex} is the externally applied excitation source. The coupled RTE system (1) can be solved to obtain the angular fluence $\widetilde{\Phi}$ at excitation and emission wavelengths.

Forward Solver: The transport equation solver for optical fluorescence modeling was developed on top of a pre-existing general purpose radiation transport analysis system Attila™ (Transpire Inc. Gig Harbor, WA, USA). Attila™ was initially developed at the Los Alamos National Laboratory [11], Los Alamos, NM, USA. In Attila™ numerical solution of transport equation involves two steps: (i) angular discretization by discrete ordinates method, (ii) spatial discretization by discontinuous finite element based differencing and the solution of the resulting linear systems with source iteration method coupled with diffusion synthetic acceleration (DSA). A high order angular quadrature set is needed to avoid ray effects in transport equation solutions for weakly scattering media. Most biological tissues are strongly scattering and a low order angular approximation provides sufficient accuracy. However, for imaging applications in which the animal is surrounded by non-scattering media and a non-contact illumination is used, a higher order quadrature is necessary to resolve the transport of excitation photons to the animal boundary. These computations can be carried out efficiently by breaking the transport calculation in two stages: (i) computing an analytical ray trace of unscattered photons through out the imaged domain, followed by (ii) a low angular quadrature based numerical transport solution with the uncollided photons acting as external sources of photons. For the imaging setup depicted in Fig. 1, the NIR source is analytically described for computing the unscattered photon flux through the animal body. The RTE solution procedure and its experimental validation is described in detail in references [12] and [13].

Inverse Solver: The general fluorescence tomography problem involves the determination of discretized fluorescence absorption coefficient $\mu_{\mathbf{af}}^{\mathbf{x}} = \{\mu_{af_i}^{x}\}, i = 1, 2...N$ from a set of discrete boundary measurements of scalar emission fluence $\mathbf{z} = \{z_j\}, j = 1, 2...M$, where z_j is defined as: $z_j = \int_{\theta_j} \widetilde{\Phi}_m^j$. θ_j is the angular aperture of the j^{th} photon collector. The measurements $\mathbf{z}$ depend nonlinearly on the unknown fluorescence absorption $\mu_{\mathbf{af}}^{\mathbf{x}}$. The tomography problem can be linearized if a first order Taylor series expansion about a initial fluorescence map $\mu_{\mathbf{af_0}}^{\mathbf{x}}$ is used to describe the boundary fluorescence measurements:

$$\mathbf{z} - \mathbf{z}_0 = \mathbf{J} \cdot \left(\mu_{\mathbf{af}}^{\mathbf{x}} - \mu_{\mathbf{af_0}}^{\mathbf{x}} \right) \quad \mathbf{J} = \left[\frac{\partial \mathbf{z}}{\partial \mu_{\mathbf{af}}^{\mathbf{x}}} \right]_{\mu_{\mathbf{af}}^{\mathbf{x}} = \mu_{\mathbf{af_0}}^{\mathbf{x}}} \tag{6}$$

Where $\mathbf{J}$ is the $M \times N$ Jacobian sensitivity matrix with M measurements and N unknowns. Calculation of $\mathbf{J}$ dominates the computational cost of typical optical tomography algorithms. Jacobian matrices for multiple frequencies are stacked to increase the available data for reconstruction. $\mathbf{J}$ can be efficiently computed by employing the adjoint transport equation. We define the adjoint system for j^{th} detector with response D_j as:

$$\begin{bmatrix} H_x^* & -B_{xm}^* \\ 0 & H_m^* \end{bmatrix} \begin{bmatrix} \widetilde{\Psi}_x^j \\ \widetilde{\Psi}_m^j \end{bmatrix} = \begin{bmatrix} 0 \\ D_j \end{bmatrix} \tag{7}$$

$H_{x,m}^*$ are the adjoint transport operators. The jk^{th} element of $\mathbf{J}$ can then be expressed in terms of the adjoint solutions $\widetilde{\Psi}_{x,m}$ by exploiting the definition of the adjoint operator:

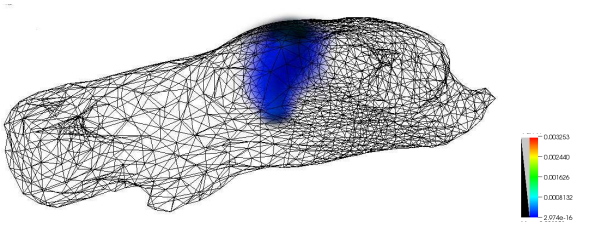

Fig. 3. Illustration of a row of **J**. The color scale indicates the sensitivity of a given source-detector pair measurement to the unknown fluorescence absorption map defined on the finite element mesh of the animal body.

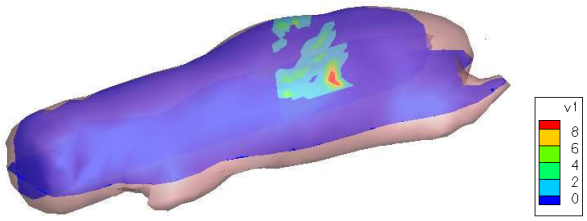

Fig. 4. Fluorescence reconstruction: Orthogonal slices drawn through the reconstructed fluorescence absorption map are depicted. The fluorescent bulb is identified.

$$J_{jk} =< D_j, \frac{\partial \widetilde{\Phi}_m}{\partial \mu^x_{af_k}} >=< \widetilde{\Psi}^j_x, \frac{\partial H_x}{\partial \mu^x_{af_k}} \widetilde{\Phi}_x > \quad (8)$$

$$+ < \widetilde{\Psi}^j_m, \frac{\partial B_{xm}}{\partial \mu^x_{af_k}} \widetilde{\Phi}_x > \quad (9)$$

The first term on the R.H.S of Equation (8) can be dropped upon invoking the Born approximation, wherein the excitation field is assumed not to be perturbed by the presence of fluorescent target. The adjoint solution $\widetilde{\Psi}^j_m$ does not depend on the particular image voxel index k, hence in a linearized tomography algorithm, the adjoint solutions $\widetilde{\Psi}^j_m$ can be precomputed and stored for all M collector locations. The **J** can then be assembled on demand provided the forward solutions $\widetilde{\Phi}_x$ corresponding to all excitation sources are available. The computation of the terms $\partial B_{xm}/\partial \mu^x_{af_k}$ depends upon the discretization scheme employed, but it is straightforward as the operator B_{xm} depends linearly on μ^x_{af}. In fact, **J** does not even need to be explicitly constructed. Iterative solution methods such as algebraic reconstruction technique or conjugate gradient least squares, only require matrix-vector products involving **J**, and they can be implemented directly with Equation (8) once the respective forward and adjoint RTE solutions are available. For the system described in Fig. 1, the pixels on the CCD images projected to the animal surface as shown in Fig. 2 are treated as detectors. Fig. 3 depicts the volume rendering of a typical row of the Jacobian matrix, with the point source illuminating the top surface.

IV. Multimodality Image Reconstruction

The projection data illustrated in Fig. 2 were inverted by means of Equation (6). For tomography, data was acquired by scanning 16 point sources on the mouse surface in transmission mode, as depicted in Fig. 1, mode a), while 213 detector points were chosen from high SNR regions on the projection images. Thus inversion required 213 adjoint RTE computations and 16 forward RTE computations per modulation frequency, however as these calculations are independent of each other, they were implemented in parallel on a Linux Beowulf cluster with 32 AMD opteron processors (2.2 GHz) and 4 GB of system memory per processor. The total time for the Jacobian computation was under 45 minutes. The forward and adjoint computations were conducted under the assumption that the entire mouse was homogeneous and the endogenous absorption and scattering cross-sections were taken to be equal to murine muscle properties reported in literature. The linear system (6) was inverted with LSQR method in MATLAB.

Fig. 4 depicts the slices drawn through the reconstructed fluorescence absorption map through the mouse body. The image resolution was limited by the coarse mesh employed to limit the computation time.

V. Conclusions and Future Work

This contribution marks our first step towards hybrid optical-CT reconstructions of small animal models with nanostructure enhanced fluorescence contrast with multi-frequency domain measurements. The weaknesses of ICG because of its low quantum yield are removed by nanoshell conjugation at the cost of decreased fluorescence lifetime, which necessitates higher frequencies ($> 200\ MHz$) for image reconstruction.

References

[1] A. Joshi, W. Bangerth, and E. M. Sevick-Muraca, "Non-Contact Fluorescence Optical Tomography with Scanning Patterned Illumination," *Optics Express*, vol. 14, no. 14, pp. 6516 – 6534, 2006.

[2] A. B. Milstein, J. J. Stott, S. Oh, D. A. Boas, R. P. Millane, C. A. Bouman, and K. J. Webb, "Fluorescence Optical Diffusion Tomography Using Multiple-Frequency Data," *Journal of the Optical Society of America A*, vol. 21, pp. 1035 – 1049, 2004.

[3] K. Hwang, J. P. Houston, J. C. Rasmussen, A. Joshi, S. Ke, C. Li, and E. M. Sevick-Muraca, "Improved Excitation Light Rejection Enhances Small-Animal Fluorescent Optical Imaging," *Molecular Imaging*, vol. 4, no. 3, p. 194 204, 2005.

[4] J. Reynolds, T. Troy, and E. Sevick-Muraca, "Multipixel Techniques for Frequency-Domain Photon Migration Imaging," *Biotechnology Progress*, vol. 13, pp. 669–680, 1997.

[5] T. Tsubono, S. Todo, N. Jabbour, A. Mizoe, V. Warty, A. J. Demetris, and T. E. Starzyl, "Indocyanine Green Elimination Test in Orthotopic Liver Recipients," *Hepatology*, vol. 24, pp. 1165 – 1171, 1996.

[6] R. C. Benson and H. A. Kues, "Fluorescence Properties of Indocyanine Green as Related to Angiography," *Phys. Med. Biol.*, vol. 23, pp. 159 – 163, 1978.

[7] C. D. Geddes, H. Cao, and J. R. Lakowicz, "Enhanced Photostability of ICG in Close Proximity to Gold Colloids," *Spectrochimica Acta Part*, vol. A, no. 59, pp. 2611 – 2617, 2003.

[8] R. Bardhan, N. K. Grady, J. R. Cole, A. Joshi, and N. J. Halas, "Fluorescence Enhancement by Au Nanostructures: Nanoshells and Nanorods," *ACS Nano*, vol. 3, no. 3, pp. 744 – 752, 2009.

[9] R. Bardhan, N. K. Grady, and N. J. Halas, "Nanoscale Control of Near-Infrared Fluorescence Enhancement Using Au Nanoshells," *Small*, vol. 4, no. 10, pp. 1716 – 1722, 2008.

[10] A. Joshi, J. C. Rasmussen, S. Kwon, T. A. Wareing, J. McGhee, and E. M. Sevick-Muraca, "Multi-Modality CT-PET-NIR Fluorescence Tomography," *IEEE ISBI*, pp. 1601 – 1604, 2008.

[11] T. Wareing, J. McGhee, J. Morel, and S. Pautz, "Discontinuous Finite Element S_N Methods on $3-D$ Unstructured Grids," *Nucl. Sci. Eng.*, vol. 138, no. 3, pp. 256 – 268, 2001.

[12] J. Rasmussen, A. Joshi, T. Pan, T. Wareing, J. McGhee, and E. Sevick-Muraca, "Radiative Transport in Fluorescence-Enhanced Frequency Domain Photon Migration," *Medical Physics*, vol. 33, no. 12, pp. 4685 – 4700, 2006.

[13] A. Joshi, J. Rasmussen, E. Sevick-Muraca, T. Wareing, and J. McGhee, "Radiative Transport-Based Frequency-Domain Fluorescence Tomography," *Physics in Medicine and Biology*, vol. 53, no. 8, pp. 2069–2088, 2008.